# OPTIMUM PLACEMENT OF HELMHOLTZ RESONATORS FOR DAMPING PRESSURE OSCILLATIONS

****

Roger M. Lloyd

Princeton University
School of Engineering and Applied Science
Aerospace and Mechanical Sciences Department

# OPTIMUM PLACEMENT OF HELMHOLTZ RESONATORS FOR DAMPING PRESSURE OSCILLATIONS

by

Roger M. Lloyd

TABLE OF CONTENTS

ACKNOWLEDGEMENTS

First the author wishes to thank the Aeronautics and Space Administration who supported this research on Contract NASr-217. The discussions with Mr. Marcus Heidmann, technical monitor on this program, were a great help in the research.

Next, the author wishes to thank the U.S. Navy for allowing him the privilege of studying at Princeton University. It has been a most rewarding and enjoyable year. The reward has been in studying under some of the leaders in the field of aeronautical engineering. The enjoyment has been in the association with the fine and friendly group of people at the Guggenheim Laboratories.

Several people rate a special note of thanks. Mr. David Harrje and Professor W.A. Sirignano were of untold help in their advice and discussions on the work. Mr. Ken Gadsby spent many hours running the equipment for the test runs and Mr. Vic Warshaw also helped occasionally on the runs and designed the testing chamber.

My thanks are also extended to Mrs. Evelyn Olsen who typed the manuscript and to the technicians and machine shop personnel who made the parts for the tests.

## ABSTRACT

Cold flow and hot firing tests were conducted to find the optimum design and positioning of an acoustic resonator for damping high intensity pressure oscillations. The variables in the cold flow tests were the position of the resonator and its volume. In the hot firings more than one resonator was used and the gas properties were also varying. Pressure node or antinode locations of the resonator were emphasized in the tests and the resonator cavity volume was varied from fully closed to three and a half times the resonant volume calculated by the Helmholtz resonator theory.

It was found that the resonator at the pressure node provided little or no damping while when positioned at the pressure antinode the sound intensity in the cold flow duct was reduced to less than 50% of the undamped amplitude. The range of damping was found to be narrow and centered around the volume calculated by the Helmholtz resonator theory. The results of the phase lag between the pressures in the cavity and duct and the velocity in the orifice, connecting the cavity and the tube closely corresponded to those predicted by Sirignano in Reference 14. An investigation of the effective length of the orifice in the Helmholtz resonator indicated that a single end correction was appropriate (rather than the double end correction for conventional acoustic amplitudes) - this also substantiated the jet flow model.

## INTRODUCTION

The combustion process in a liquid propellant rocket engine is never completely steady. There will always be random fluctuations in the propellant burning due to the differences in time necessary for each droplet to vaporize, diffuse and then burn. Each of these processes depends on certain physical factors such as mixture ratio, pressure, temperature, and velocity of the gases in the combustion chamber. All of these factors are time dependent so absolutely uniform combustion would not be expected. Since fluctuations are random throughout the chamber, the mechanical stresses on the walls of the chamber and changes in heat transfer would be only slightly affected. Random pressure fluctuations which do not exceed a value greater than plus or minus five percent of the mean chamber pressure are normally classified in the category of rough combustion.[1]

If the fluctuations are not random, but are periodic, then the oscillations at one point will be related to those at other points in the chamber. These oscillations can be of the spontaneous type, i.e., with a slow build-up out of the combustion noise, or of the nonlinear type where a disturbance (trigger) would be responsible. The oscillations will increase in intensity causing thermal and mechanical stresses, which, if left unchecked, could ultimately lead to the destruction of the motor.

In general there are three ranges of frequency for instability. There is the low frequency range which is of the order of 10 to 200 Hz, the high frequency range with frequencies normally greater than 1000 Hz, and the intermediate range which is of the order of several hundred Hz.

The low frequency instability is usually feed system coupled and is often referred to as "chugging".[2] The propellant requires a time lag to mix the propellants and absorb the energy necessary to initiate combustion. The coupling of the feed system and combustion results in the variation of flow rate with time. This in turn causes the chamber pressure to oscillate, sometimes with considerable amplitude.

These oscillations may build until the rocket motor fails. Low frequency instability is usually fairly easily controlled by relatively simple methods such as increasing the injection pressure drop and hence this type of instability seldom causes major problems in the final hardware.

Combustion oscillations with frequencies between those of low and high frequency instabilities can be caused by a variety of coordinating processes. They may involve mechanical vibrations of the structure of the engine, characteristic frequencies of the injection mechanism, resonances of the feed lines, eddy patterns set up by flow around sharp edges or through complicated channels, or even various flow disturbances caused by high heat transfer rates. Most of these intermediate range types do not reach very high amplitudes. However, they often cause lowering of performance rather than destroying hardware. The intermediate range oscillations are often referred to as buzz instability and at times as entropy waves.[3]

The high frequency instabilities are located in the rocket combustion chamber and often have practically no effect on the propellant flow rates due to the inertia of the propellant in the lines. However, the heat transfer from the gas to the walls can be increased by a factor as high as 10 times normal. The frequency of the instability is dictated by the geometry of the chamber and the combustion characteristics of the propellant. The frequency is inversely proportional to the length of the chamber for long motors. As the thrust level is increased and the ratio of length to diameter decreases, it is found the diameter becomes the more important factor in determining the high frequency oscillations which will be present. The waves are longitudinal in small diameter rockets and progress to transverse oscillations which may be radial or tangential as the diameter becomes the dominant length. The high frequency instability is the most destructive form of instability because its peak-to-peak amplitude may be as great as several times the mean chamber pressure causing structural failure of the chamber.[4] The associated heat transfer rate increase is even more critical and normally causes chamber failure due to local

and/or overall heat transfer excesses.

The waves formed could be of any frequency compatible with the geometry of the chamber and combustion characteristics of the propellants. However, normally the lowest modes are preferred. Even with this preference it is often difficult to suppress such high frequency instability.

One method of achieving stability as well as frequency control is afforded by baffles. Baffles can be of many shapes and sizes but all have the common purpose of damping out transverse instabilities. The number of blades determines which tangential modes can be controlled. It has been found in tests by many investigators that the baffle should be placed in the sensitive zone of the combustion which extends from the injector face perhaps as far as five inches downstream.[5] For efficiency, baffle compartments are often designed to an odd number since acoustic patterns require a nodal line that separates regions of high and low pressures. The baffle thus fixes the mode (i.e., a three-bladed baffle would still allow a third tangential standing mode to exist between the blades).

Once the mode of the instability has been fixed the possibility of achieving stability is enhanced. Another method for achieving stability, this time via a damping approach, is to use an acoustic liner and/or tuned acoustic resonators to remove the energy from the pressure waves. For small oscillations the Helmholtz resonator formula is used to find the cavity resonant frequency, but for larger amplitudes there may be a significant deviation from this value. The Helmholtz resonator is very limited in its frequency band, therefore to achieve an efficient design the instability modes must be restricted, a task which the baffle performs well. The placement of the resonators at pressure nodes or antinodes is another matter. This experimental work follows preliminary studies at Princeton involving the optimum placement of the acoustic resonators around the circumference of the motor.

## THEORY

The computation of the acoustic frequencies for a motor is a simple matter and is governed by the solutions to the classical wave equation. However, since the oscillations observed during combustion instability are frequently of large amplitude relative to that normally considered for acoustic theory, the apriori applicability of the wave equation under such conditions is open to question. Nevertheless, it has been found that experimental observations in such cases are surprisingly well described by classical acoustics.[6]

The wave equation for a pressure disturbance $p$ is given by:

$$\frac{\partial^2 p}{\partial t^2} = c^2 \left[ \frac{\partial^2 p}{\partial x^2} + \frac{\partial^2 p}{\partial r^2} + \frac{1}{r} \frac{\partial p}{\partial r} + \frac{1}{r^2} \frac{\partial^2 p}{\partial \theta^2} \right]$$

By separating variables and proper selection of boundary conditions this wave equation can be solved into a Bessel function solution which yields a relationship for frequency of all natural modes of the chamber cavity.

$$f_{m,n,q} = \frac{c}{2} \sqrt{\left(\frac{a_{mn}}{R}\right)^2 + \left(\frac{8}{L}\right)^2}$$

where: $a_{mn}$ = $n^{th}$ root of $J_n$ Bessel function of the first kind.

$c$ = speed of sound in the medium

$L$ = length of the cavity

$m, n, q$ = wave numbers

The wave numbers $m$, $n$, and $q$ correspond to all possible modes of acoustic oscillations within the cavity. When only one of these is not zero the corresponding mode is called pure. The pure modes are $m \neq 0$, tangential, $n \neq 0$, radial, and $q \neq 0$, longitudinal. Modes corresponding to more than one non-zero wave number are called combined or mixed modes.

When baffles are used to fix the frequency of the oscillations, it would be possible to get many frequencies which are compatible with the baffle configuration. For odd numbers of blades, the tangential mode which corresponds to the number of blades or some higher multiple harmonic is available (i.e., for a three-bladed baffle the third, sixth, ninth, etc. tangential modes are possible). However, for an even number of blades it is possible to get the mode corresponding to half the number of blades and the higher harmonics (i.e., for a four-bladed baffle the second, fourth, sixth, etc. tangential modes would be available). In practice, the higher harmonics do not usually appear in the smaller motors because their frequencies are too high for combustion support, while in the larger motors modes to the fourth tangential have been observed (i.e., in these chambers frequencies are still not too high for combustion coupling).

The problem of instability is so complex that no exact theory is possible. However, analytical models can provide insight into important aspects of the phenomena. These models attempt to describe the major processes and variables that occur and are present in the combustion chamber. It is normally assumed that some one process such as the vaporization, mixing or chemical reaction is much slower than the other processes and therefore is the rate-controlling step. By doing this it is assumed that the rate-controlling step represents a major part of the characteristic time during which coupling can occur and by neglecting the other processes only a negligible error is introduced.

Most analytical combustion models start by combining the conservation equations into the generalized wave equation. Pressure disturbances are then introduced into the wave equation and solutions are made to determine if the pressure amplitude of the disturbance grows or decays with time. Solutions to the neutral wave equation represent cases where a pressure disturbance neither decays nor grows and as such corresponds to stability boundaries which separate regions

of stable and unstable operation. The addition of a forcing function can cause the pressure amplitude to increase, whereas, the addition of a damping function will cause it to decrease. The models of the forcing functions are based on the chemical and physical properties of the propellant and rocket chamber.

Combustion models are treated using either a linear or nonlinear approach. The linear approach eliminates all higher order terms from the wave equation and considers the amplification of small perturbations which can lead to other processes. In this sense the linear model is concerned with the initial phases in the transition from a small disturbance to instability. These instabilities can be considered as those which seem to grow out of the combustion noise into a sustained oscillation. The nonlinear approach is concerned with the transition from a finite disturbance to a large amplitude disturbance.

There are presently two widely accepted models of instability. They are the Crocco Sensitive Time Lag Model[7,8,9,10] and the Priem Theory[11]. The sensitive time lag theory is a linear analysis which assumes the perturbations are sufficiently small so that all terms higher than linear in the perturbation expressions can be neglected. Each of the quantities describing the flow in the combustion chamber is assumed to oscillate about a given steady-state value. By finding the existence of neutral oscillations which neither grow nor decay, the boundary between stable and unstable regions is found for each acoustic mode. Sirignano and others at Princeton have more recently extended the time lag theory and looked into the nonlinear aspects as well.

The sensitive time lag theory says that the combustion process can be represented by a total time lag, $\tau_t$, so the final products of combustion pertinent to a given element of injected propellant are developed instantaneously after a well-defined time from the moment of injection. The use of a time lag permits one to ignore the details of the combustion process. Crocco further represented the total time lag

as the sum of the constant insensitive time lag $\tau_i$ and the sensitive time lag $\tau$. The sensitive time lag depends on local combustion chamber conditions and therefore in reality it can be different for each element of propellant injected. However, for simplicity, an average sensitive time lag value is normally assumed. The time lag varies with time and responds to fluctuations in the combustion chamber conditions. The sensitive time lag must be close to half the period of the harmonic frequency so that energy from the combustion will be added in such a way as to increase the amplitude of the instability. Energy added in phase with the instability will increase the amplitude. If the frequency of the mode is too high the energy will not be added in phase and will not support the instability. Thus, if the combustion is altered so that this sensitive time lag is decreased from a stable value the initial coupling would be with the lowest frequencies possible in the chamber (first tangential, first longitudinal, etc., depending on the chamber dimensions). If the time lag was decreased further the higher modes would then be favored. For simplicity, it was first assumed that all such fluctuations could be correlated to local pressure. Later velocity effects were added to the theory.

An interaction index is defined by the theory as a measure of the relative magnitude of the coupling between the combustion process and the chamber harmonics, the larger the interaction index the better the coupling while below a certain minimum value no coupling can occur. It is further postulated that the interaction index varies during the time lag, being small initially and attaining its largest values just before the conversion to combustion products. The analysis approximates this variation of the time index by a step function which divides the total time lag into two parts. During the insensitive part the index is zero and during the sensitive part it has a constant positive value.

Considering only small perturbations, and solving the wave equation, yields the following expression for a stability boundary:

$$A\nu\eta^n \left(1 - e^{-i\omega\tau}\right) = h(\omega)$$

where $\omega$ is the frequency of oscillation.

The left side of this equation represents the energy supplied by the combustion process which must be completely absorbed by the fluid mechanical process represented by $h(\omega)$ on the right side. If more energy is supplied than can be absorbed, the oscillation amplitude will grow.

The Priem nonlinear combustion instability model uses a one-dimensional model of the combustion chamber for determining instability limits. The theory solves the nonlinear conservation equations with mass addition using a steady-state expression for the burning rate. Droplet vaporization is treated as the rate-controlling process. Therefore, it applies only if at least one component of a bipropellant system has a slow vaporization rate. Priem's results were valid only for large droplet-gas relative velocities or large droplet Reynolds number.

Combustion instability zones are determined by combining the nonlinear instability model with a steady-state vaporization program. The analysis determines the zones in which the tangential modes of high frequency instability can be most easily initiated. It also predicts the most sensitive point in the combustion chamber to be at the position where the difference in velocity between the gas and droplet is zero.

The use of mechanical damping devices to control instability has followed two principal paths: the baffle approach and the liner approach. In the latter, the acoustical absorbing wall consists of a perforated liner separated by a volume of gas from a solid wall or pressure vessel. For the case of sound intensities in the normal acoustic regime, the mass of gas in the liner aperture and the volume of gas in the cavity behind the liner form an oscillating system that is analogous to a spring-mass system.[11] This system has the typical frequency response of a damped oscillator. Energy dissipation is predominantly due to viscous losses for low amplitude waves and occurs through oscillation of the gas in the apertures of the liner. At high incident amplitudes, turbulence and circulation due to high particle

velocities in the liner apertures effectively control the absorbing characteristics. The absorption coefficient is defined as that fraction of the incident wave energy that was absorbed. It is made up of two contributions; that of the acoustic resistance and that of the acoustic reactance. The acoustic resistance is that component of acoustic impedance associated with the dissipation of acoustic energy within the aperture of the liner. The specific acoustic resistance is a function of the gas properties within the aperture, the liner parameters, and the acoustic energy dissipation losses.

$$\bar{\theta}_o = \frac{4}{\sigma \rho c} \left(\frac{\pi \mu \rho f_o}{g}\right)^{\frac{1}{2}} (1 + t/d + \Delta n \ell/d)$$

The terms $\ell$ and $t/d$ represent the viscous losses on the facing and within the apertures of the acoustic liner respectively, and the $\Delta_{n\ell}/d$ term represents the nonlinear loss due to intense sound (i.e., sound levels beyond the scope of the acoustic theory).

The second component of the acoustic absorption is that of the acoustic reactance, which is the component of acoustic impedance associated with the effective mass and stiffness of the acoustical system. The reactance is primarily a function of the effective aperture length, the liner open area ratio, and the frequency ratios between the chamber oscillation frequency of interest and the aperture resonant frequency.[12]

$$\bar{x} = \left(\frac{2\pi f_o \ell_{eff}}{c\sigma}\right) \left(\frac{f}{f_o} - \frac{f_o}{f}\right)$$

where $\ell_{eff} = t + 0.85\, d(1 - 0.7\sqrt{\sigma}) - \delta$ is the effective length,*

$c$ = speed of sound

$t$ = liner thickness

$d$ = aperture diameter

$\sigma$ = open area ratio

$\delta$ = arbitrary correction factor

$\mu$ = viscosity of gas in the orifice

$\rho$ = density of gas in the orifice

---

* $\ell_{eff}$ as defined by this relationship has a double end correction.

It has been found that the linear terms of the acoustic resistance predominate below sound levels of 130 db and the nonlinear term becomes a major factor above 140 db.[13] Since the area covered in this report is well above the 140 db level, being in the 180 to 200 db range, we assume the nonlinear dissipation of energy is due to the jet breakup at both ends of the orifice and the turbulence produced in the chamber due to the interaction of the jet with the chamber flow should dominate over the linear dissipation.

The natural frequency of a resonator configuration is the frequency at which the resonator offers no specific reactance to the sound wave. The frequency at which this occurs is known as the resonant frequency and it may be expressed as follows:

$$f_o = \frac{c}{2\pi} \sqrt{\frac{\sigma}{L \ell_{eff}}}$$

where L = cavity height.

For operation at off resonant frequency conditions it has been found by Blackman and others that the reactance increases with frequency and decreases slightly with increasing sound pressure level.[12]

Sirignano has developed a model for use in an analytical study of the flow field associated with an acoustic liner.[14] His analysis is based on the following assumptions:

1. There is no mean flow through the orifice.

2. The loss due to separation at the orifice tube entrance is neglected while the exit loss is set equal to the kinetic energy of the flow in the jet.

3. One-dimensionality may be assumed for the flow through the orifice with shear in the boundary layer averaged over the cross-section.

4. The unsteady boundary layer is small compared to the diameter of the orifice so that flat-plate results may be used to calculate the friction on the wall.

5. The length-to-diameter ratio of the orifice is sufficiently high to consider the flow just outside the orifice to be quasi-steady.

6. The amplitude of the velocity oscillations is sufficiently higher than the critical velocity for separation and jet formation so that the portion of time in the cycle when potential flow occurs as the velocity goes through zero is negligible when compared to the period of the cycle. Therefore, it is reasonable to consider the flow is always separated.

7. The orifice length as well as the cavity dimensions is considered very small as compared to the wavelength of the oscillations.

8. The entropy and mean temperature of the cavity gas remains constant with time even though dissipation in the jet occurs. This is reasonable if the chamber volume is much larger than the product of the root mean square of the flow rate and a characteristic observation time of interest such as the damping time. Also, of course, the portion of heat transferred to the walls due to the oscillations must be negligible. If these assumptions about entropy and mean temperature can be made for the cavity gas, they should also be reasonable for the gas in the much larger combustion chamber.

9. Only the oscillating pressure in the chamber is considered. Neither is the effect a mean flow in the chamber past the orifice considered.

10. The amplitude of the oscillations are not so large as to cause choking of flow through the orifice at any instant of time.

By employing the concept of conservation of momentum and relating the pressure in the cavity to the mass in the cavity and further relating that to the mass flux through the orifice one finds

$$\rho_2 u_2 A = \frac{d}{dt} (\rho_{II} V) = \bar{\rho} V \frac{d}{dt} \left(\frac{p_{II}}{\bar{p}}\right)^{1/\gamma}$$

where bar superscripts denote steady-state quantities, subscript 2 denotes conditions at the cavity end of the orifice, subscript II

denotes stagnation conditions several diameters from the orifice in the cavity and $V$ is the volume of the cavity.

By making use of assumption 5 to relate the pressures near the orifice to those away from the orifice, a method of successive approximations gives the first order velocity

$$u^{(1)} = \frac{V}{\gamma A \bar{P}} \frac{dP_{II}^{(1)}}{dt}$$

where the superscript in parenthesis is the order of the approximation. For the second order approximation

$$\bar{P} \frac{d}{dt} \int_o^{\ell} u^{(2)} dx = P_I - P_{II}^{(2)} + \tau/A - \frac{d}{dt} \int_o^{\ell} \rho^{(1)} u^{(1)} \, dx \pm \frac{\gamma \bar{P}}{2} \left[ \frac{u^{(1)}}{\bar{c}} \right]^2$$

where the $+$ represents flow into the cavity and $-$ is flow out and

$$\frac{d}{dt} \frac{P_{II}^{(2)}}{\bar{P}} = \frac{\gamma A}{V} \left[ u_2^{(2)} + \frac{P_{II}^{(1)}}{\bar{P}} u_2^{(1)} \right]$$

The solution of these two equations for $P_{II}^{(2)}$ and $u^{(2)}$ contain particular solutions of two types: those related to the dissipative effects represented by the friction term $\tau/A$ and the exit loss $\pm (\gamma \bar{P}/2)(u^{(1)}/\bar{c})^2$, and those that are due to inhomogeneous terms not related to dissipative effects. The particular solutions of the latter type merely modify the solution by producing harmonics or constants other than the harmonic obtained in the linear solution so they are disregarded. The particular solutions of the first type modify the harmonic obtained from the linear solution and are most important. Using these solutions it was found that the solutions for $u^{(2)}$ and $P_{II}^{(2)}$ which exclude the higher harmonics are functions of the velocity amplitude and phase angle. Solutions for the velocity amplitude and phase angle are then found.

The Sirignano theory predicts, for frequencies much higher than the resonant frequency, the duct pressure will lead the orifice

velocity by 90 degrees and the cavity pressure by 180 degrees. For frequencies much lower than the resonant frequency, the duct pressure will lag the orifice velocity by 90 degrees and be in phase with the cavity pressure.

## GENERAL DESCRIPTION OF THE APPARATUS

The purpose of the experiment was to find the damping effect of an acoustic resonator on fairly high intensity waves. The intensity of the waves had to be over 140 db so the nonlinear damping terms would play a major role. The variables were to be acoustic resonator volume, resonator position and the frequency of the impressed wave.

To accomplish the design goals a duct was used which could be placed in longitudinal mode resonance via a siren placed at the end. The test section, incorporating the Helmholtz resonator, could be moved through a quarter wave length for frequencies in excess of 273 Hz. This enabled evaluation of resonator operation at both pressure node and antinode locations. A piston-like arrangement allowed the resonator to be tuned over a wide range above and below the design value ($V/V_{res}$ from 0 to $> 3.5$).

The details of the apparatus are shown in Figure 1. The high pressure air (from a supply which was nominally 2000 psig) was passed through a thermostatically controlled water bath to ensure a constant temperature supply of air to the remainder of the system. The air then passed to a 0-500 psig regulator which fed the upstream side of a calibrated sonic orifice. A copper-constantan thermocouple and a static pressure tap leading to a bourbon-tube gage were just upstream of the orifice to allow calculation of the mass flow. The flow then passed into a plenum chamber and then into the 9 ft. length of 1.5 in. I.D. duct in which the oscillations were introduced. The average static pressure in the duct was measured at the upstream end by a bourbon-tube gage. A restriction in the line at the pipe enabled the gage to take an average pressure reading under oscillating conditions. A copper-constantan thermocouple in the duct measured the air temperature so the physical properties of the air passing into the test section were known and the velocity in the duct could be determined from the known mass rate of flow. The test section was mounted flush with the flanged ducting (1.46 inch I.D. and 1.50 inch O.D.) using static

O-ring seals (Figure 1). The 1.50 inch O.D. duct was telescoped into flanged sections of 1.50 inch I.D. duct using dynamic O-ring seals. The inner duct and test section was traversed using a "zeromax" variable speed motor which drove a worm gear, mounted parallel to the duct, through a flexible coupling. The aluminum frame, together with the test section assembly, moved (on sliding bearings) on two rods mounted parallel to the duct. The "zeromax" motor was operated from the main control panel through a relay system. The range of longitudinal positions accessible was about 17 inches which allowed placement of the acoustic resonator at a pressure or velocity node or antinode. The longitudinal position of the test section was monitored on the control panel through an ammeter with two potentiometers mounted on the control panel to allow the extreme upstream and downstream positions of the test section to be set on the meter. Limit switches prevented the test section from running into the flanged ducting on the ends of the movable section.

The test section, shown in Figure 2, was a 3 inch long, 4½ inch O.D. brass block with a 1.46 inch diameter hole forming the duct. A 0.3 inch diameter orifice was drilled in from the side and a variable volume acoustic resonator chamber attached. The mounting of the acoustic resonator required a flat surface so one side of the brass rod was flattened leaving the orifice 1.27 inches long. A 6¼ inch long, 1.5 inch I.D., steel tube, with 0.25 inch walls, was mounted on the flattened side, centered over the orifice, to provide the walls of the acoustic cavity. The seal was provided by an O-ring and four threaded steel rods which screwed into the brass block at one end and passed through an aluminum plate above the chamber where they were held in place by nuts. The aluminum plate was a mounting for the piston position indicator, gears to operate the piston, the motor for piston operation, and limit switches to stop the piston at its travel limits. The motor used for positioning was a 115 volt a.c., 1725 rpm, 1/70 hp, "Bodine" motor. It ran a spur gear through a direct coupling. This gear in turn operated another spur gear which

ran a threaded rod in and out to position the piston in the steel tube. The gear also operated a mechanical counter which was viewed from the control room with a telescope to determine piston position. The piston, which was used to vary the chamber volume, was made of brass and the cavity was sealed with an O-ring. A Kistler model 601A pressure transducer was mounted flush with the face of the piston with the wire passing through the piston and out a 1/2 inch diameter hole in the side of the tube wall 3/4 inch from the top of the tube.

A second Kistler model 601A was mounted flush with the wall of the duct at a position $90^{o}$ from the orifice entrance. Hot wire probe openings were located opposite the orifice in the duct and at four positions in the orifice so that the velocities in the duct and orifice could be observed.

The pressure oscillations were introduced through the use of a siren which was placed a few thousandths of an inch from the end of the duct. At the end of the duct was a variable area nozzle assembly with the opening controlled remotely. The siren together with the variable nozzle assembly served as the nozzle throat which changed in area as the siren wheel rotated. This area change caused the oscillating component of the flow and the inter-orifice gap (between the downstream surface of the variable area nozzle assembly and the siren wheel) controlled the strength of the oscillations. The siren wheel was driven through a timing belt system by a 15 hp, U.S. Electric Motors "vari-drive" motor. This motor consisted of an electric motor which could be driven at two different constant speeds, a system of two variable width pulleys and a belt, a gearbox and control equipment. The output speed of the motor was adjusted by operating a small electric speed-change motor which changed the widths of the pulleys. The direct output of the motor gearbox was variable over a speed range of about 8 to 1. The timing belt system provided additional speed reductions of 1:1, 3.43:1, and 11.76:1. Various siren wheels with 2, 4 and 28 holes could be used to give a siren frequency range of roughly 5 to 5000 cps.

A Dynisco pressure transducer (model PT 76-1M, 0-1000 psig) was mounted just upstream of the variable area nozzle. This transducer is of the strain-gage type, four-arm bridge, with two windings wound circumferentially and two windings wound axially on a strain tube mounted between the diaphragm and the backing plate. The bridge was excited with a Video Instruments model SR-200-EHM D.C. power supply set to 10 volts. The output of the bridge was fed to a Dana model 2200 operational amplifier set to a gain of 1000.

The outputs of the Kistler pressure transducers in the duct and piston head were fed into Kistler charge amplifiers set on the 5 psi/volt range and 0.5 psi sensitivity. The outputs of the Kistler charge amplifiers, the Dana amplifier, and the hot-wire anemometer were fed into a Tektronix dual-beam oscilloscope for display. Pictures were then taken with a Hewlett Packard oscilloscope camera using black and white 3000 ASA speed Polaroid film.

The hot wires were made of 0.15 mil. tungsten wire with a 0.04 inch bare area. The wires must be aligned perpendicular to the flow since they measure the velocity by keeping a constant resistance (which maintains a constant temperature) and therefore the wire current (in this case equivalent to the wire voltage) varies with the cooling of the air stream. The velocity varies approximately as the square of the difference of the square of the current and the square of the current at zero velocity as shown by King's equation in Reference 15.

(1) $P = I^2R = (A+B\sqrt{V})\ (t_s - t_e)$

$P$ = electrical power input from sensor to circuit

$V$ = flow velocity

$t_s$ = sensor surface temperature

$t_e$ = fluid temperature

A and B are constants depending on fluid properties as shown in Ref. 4

$A = 0.42\pi k_f\ L\ Pr_f^{0.20}$

$B = 0.57\pi k_f\ L\ Pr_f^{0.33}\ (d_o/\nu_f)^{0.50}$

where:

$k_f$ = thermal conductivity of the fluid

$L$ = sensor length

$Pr_f$ = Prandtl No. = $\mu_f C_f / k_f$

$\mu_f$ = kinematic viscosity of fluid

$C_f$ = specific heat of fluid

$d_o$ = sensor diameter

$\nu_f$ = dynamic viscosity of fluid

f = subscript indicating that fluid property values are chosen at the average of sensor temperature and fluid temperature

After carrying out the mathematics this becomes:

$$(2) \quad (I^2 - I_o^2)^2 = kV$$

The output from the hot-wires was fed to a "Heat-Flux System" constant temperature anemometer (model 1000A) through a special coaxial cable also manufactured by Thermo Systems, Inc. The output from the anemometer was fed into the oscilloscope for display and also into the Leeds and Northrup potentiometer for the voltage reading to determine the velocity.

The procedure for the runs entailed bringing the siren up to speed, and obtaining the correct flow rate by adjusting the upstream and downstream pressures. The speed of the siren, and thus the impressed frequency, was adjusted to give a maximum reading on the Dynisco pressure transducer at the end of the duct. This assured that the impressed frequency was a duct resonant frequency. The traversing section was then moved until a maximum or minimum was found in the peak-to-peak duct pressure oscillations. In this manner the pressure antinode or node position was established for the resonator. Oscilloscope photographs were taken of the pressure oscillations at the end of the duct,

in the duct, and in the acoustic resonator cavity together with the velocity in the duct and orifice. The piston was then moved from the zero position (negligibly effective position) to increase the resonator cavity volume in increments of one-half the calculated resonant cavity volume for the frequency used. The test was then repeated. In the tests where the interaction between the duct and resonator were taken into account the maximum unsteady pressure amplitude was separately achieved at each test point.

## DISCUSSION OF TESTS

The initial tests were made assuming that the natural frequency of the duct would not be significantly affected by the small added volume of the acoustic resonator. The 13th harmonic (417 Hz) of the natural frequency of the tube was selected since the piston travel allowed in the apparatus design was limited thus limiting the volume of the resonator cavity. With this arrangement a sufficient range of cavity volumes above and below resonance was possible (i.e., $V/V_{res}$ ranging from 0 to 3.5).

As pointed out by Heidmann, the addition of the resonator volume could alter the natural frequency of the duct itself necessitating a frequency check each time the volume of the cavity was changed. This was checked and although there was only a small change in the overall results, specific results, such as the location of the point of maximum damping, were definitely influenced.

The tests clearly showed that the placement of the acoustic resonators in specific positions on the circumference of a rocket motor is very important. The placement of the resonating cavity at the pressure antinode position reduced the peak-to-peak amplitude of the pressure at the end of the duct by about 50 percent when the cavity was tuned to the calculated resonant frequency as shown in Figures 3 through 5. The positioning of the resonator cavity at the pressure node position showed very little if any effect on the pressure at the end of the duct as may be seen in Figure 5. The pressure antinode positions may be established by means of baffles with the resonators being placed near the blades.

The tests run with a point-by-point resonance adjustment are shown in Figures 3 and 4. Figure 3 illustrates two methods of determining the resonant cavity volume. The first is based on the location of the lowest r.m.s. (in this case at the duct pressure recorded in the duct pressure recorded in the duct end but the same pressure is measured at the test section). This is the point of maximum damping.

The second approach involves the determination of the point of pure resistance (i.e., $90^{o}$ phase lag between cavity and duct) which is shown to occur at the same $V/V_{res}$ point. It is of interest to note, even with the scale used on the abscissa of this figure, that the maximum damping point occurs at a point other than that determined by $\ell_{eff}$, the double-end correction length.

Figure 4 provides data on the exact location of the maximum damping. Here the effect of constant frequency testing versus point by point resonance checks is shown. While the constant frequency case would imply a design with an $\ell_{eff}$ even greater than that with a double-end correction, the point-by-point method shows that the length is midway between the double-ended and no end correction cases. This single end correction would allow for an inlet flow correction with a jet exit - exactly the physical picture of the damping model used by Sirignano.[14]

Returning to the phase data presented in Figure 3, the $90^{o}$ lag means that there is pure resistance and no reactance present. The lag is less than 90 degrees when the cavity volume is less than that calculated by the Helmholtz resonator theory and greater than 90 degrees when the volume is greater than that calculated. Once the volume was doubled there was little effect on the phase relationship between the cavity and duct pressures with any additional volume increase. Actually the experimental data indicate asymptote of approximately $160^{o}$. The lag is less than 90 degrees when the volume is less than that calculated by the Helmholtz resonator theory may be interpreted as a more rapid loss in resistance than gain in reactance thus causing lower impedance. For the lag of greater than 90 degrees, the reactance is increasing faster than the resistance is decreasing so the impedance is increasing. The tests showed that the duct pressure led the orifice pressure by 60 degrees instead of 90 degrees and the cavity pressure by 160 degrees instead of 180 degrees, for the frequency much higher than resonant frequency, as was predicted by Sirignano. This is due to some reactance being present which is not

predicted by Sirignano's theory since he uses only the first harmonic of the velocity in the orifice. At the low frequency end where the frequency is much lower than the resonance frequency, the duct pressure lags the orifice velocity by only 70 degrees and is in phase with the cavity pressure. Again the experiments were close to the Sirignano prediction that the duct pressure would lag the orifice velocity by 90 degrees and be in phase with the cavity pressure.

Another measurement within the resonator cavity that is of interest is the cavity pressure. Figure 6a compares the peak-to-peak pressure amplitude for the cavity ($k_1$) and for the duct ($k_2$) . As previously mentioned, the duct pressure at the test section duplicates the behavior of the duct end reading. That the factor relating pk-pk to r.m.s. is close to $2\sqrt{2}$ (i.e., 2.83) is indicative of the sinusoidal nature of even this relatively high amplitude pressure wave (190 Db level). The peaking of the cavity pressures at $V/V_{res}$ ratios less than 1 (i.e., from the cavity standpoint frequencies less than the design frequency are as predicted. However, only through a new series of tests in which the duct unsteady pressure ($k_2$) is maintained constant would the final proof be obtained. Such tests require alteration of the inter-orifice gap to maintain $k_2$ constant.

Figure 6b shows how the records from constant frequency tests also verify the trends from Figure 6a. Small variations in inter-orifice gap settings account for the spread in data.

The velocities in the orifice and duct depicted in Figures 7 and 8 are r.m.s. values and are nearly constant once the volume is larger than one-half the resonant cavity volume. The velocity into the cavity is higher than the velocity out until the resonant cavity volume is reached as may be seen in Figures 9 through 16. After the resonant cavity volume has been reached, the velocities in and out of the cavity are nearly the same.

The phase lags shown in Figures 17 and 18, of the velocity into the cavity as compared to the duct pressure, and velocity out of

the cavity as compared to the cavity pressure were nearly the same for all tests. The phase lag of the velocity into the cavity was about 15 degrees more than would be expected when the cavity volume was less than the resonant volume. The phase angle rapidly approached 60 degrees when the volume was increased beyond the resonant cavity volume and remained constant. The phase lag of the velocity out of the cavity is shown in Figure 18. The phase lag increased as the cavity volume increased up to one and a half times the resonant volume. It then dropped at two times the resonant volume and returned to a higher level above two and a half times the resonant cavity volume.

The method of measuring the phase lags and the amplitudes referred to in the discussion are depicted in the Figures 9-16 where the original oscilloscope photographs are marked appropriately.

# APPENDIX A

## CALIBRATION OF HOT-WIRES

Each of the two, 0.04 inch bare length, 0.15 mil diameter, tungsten wires was placed in the center of the duct with the traveling test section in the extreme downstream position, so that the hot-wire was located approximately 49 diameters from the duct inlet. A 0.200 inch diameter calibrated sonic orifice was used and the pressure upstream of the orifice was varied from approximately 393 psia to 124 psia to give a velocity range of from approximately 85 to 25 feet per seond when a uniform velocity was assumed across the duct.

The velocity obtained by using the mass rate of flow and downstream conditions, called the average velocity, must be corrected for the discontinuity of flow in the duct due to the viscosity of the fluid. In Reference 17 a chart of average velocity over maximum velocity is plotted against Reynolds number. The values on the chart were used to obtain the centerline velocity for the hot-wire calibration.

The cold resistance of the wire was found by measuring the resistance of the wire, probe, and cable from the apparatus to the hot-wire anemometer, and subtracting the known cable and probe resistances. The cold resistance was multiplied by 1.5, the overheat ratio, which was arbitrary, to obtain the hot resistance. The resistance of the cable and probe was then added and the total hot resistance was set on the Heat Flux System's hot-wire anemometer by using the probe resistance dials. The hot-wire anemometer was then placed in the run mode and the bridge was balanced by putting the toggle switch on bridge balance and turning the balance knob until a null was obtained on the null indicator. The bridge voltage was then read by using the Leeds and Northrup potentiometer. The current in the hot-wire was then found by dividing the bridge voltage by the sum of the bridge resistance and the total hot resistance set on the hot-wire anemometer. A plot was then made of the velocity computed from the mass rate of flow with Reynolds number correction and the current. The results are shown in Figure A-1.

## APPENDIX B

## RESONATOR TESTS USING LIQUID ROCKET MOTORS

The work described in this report was a continuation of previous work described in detail in Reference 18. Tests were made in an attempt to use a limited number of acoustic resonator cavities to bring dynamic stability to an otherwise nonlinearly unstable system. Liquid oxygen and ethanol were used as propellants in a 9-inch diameter rocket with a heat sink chamber using 16 spuds of like-on-like or unlike doublet design arranged on an 8-inch diameter with thrust levels of about 1300 pounds. Chamber pressures were nominally set at 150 psia through the choice of nozzle throat size and flow rates. Pulsing was achieved by use of tangentially oriented pulse guns and the first tangential mode instability of 250 psi peak-to-peak amplitude was observed following a tangential pulse when spuds of like-on-like design were used.

The acoustic dampers were acoustically tuned cavities placed at three distances downstream from the injector face (0.75, 2.00, and 3.25 in.) in the chamber wall. There were eighteen cavities at each downstream position with equal spacing radially around the chamber and the middle ring off-set $10^{o}$ from the other two rings. The orifice for each cavity was composed of six, 0.50 in. long, 0.100 in. diameter, orifices entering the cavity. It was found that damping was accomplished with as few as three active tuned resonating cavities spaced at $120^{o}$ intervals around the liner. The time to damp was short, being of the order of 25 milliseconds for nine active cavities and 17 milliseconds for 27 active dampers. The cavity volume could be increased to approximately three times the calculated resonant volume before marginal damping was experienced. Design frequency of 60% of that desired could still provide stable operation. Thus, for this chamber-injector configuration, only a limited number of acoustic resonators were necessary and these provided damping over a sufficient band to eliminate the finite disturbances encountered.

Certain injector arrangements, where the propellant flow was made circumferentially non-uniform, caused standing modes which often avoided the locations where optimum damping was provided via the resonating cavities. Hence, baffles were used to control the modes and maximize the damping. It was found that with such a three-bladed baffle the instability was damped in less than 10 cycles and hence, it was difficult to maintain instability for testing damper effectiveness. The mixture ratio variations (and hence temperature striations) were apparent from marking on the aluminum oxide chamber wall coatings. Cavity measurements indicated an out of resonance condition immediately following the passage of the high amplitude wave. Actual conditions were sometimes far from those assumed in the design. For example, in one case the cavity frequency was initially depressed more than 10% and required 10 cycles to reach nominal frequency (2780 Hz). Beyond that point there was a phase lag of $138^{o}$ across the orifice. If the phase map constructed from the nonlinear flow behavior model discussed in Reference 18 were used, the implications were that the cavity temperature was only of the order of $600^{o}R$, even after a regime phase reading had been reached. Another cavity in the same test had a phase lag of only $78^{o}$ which would be representative of about $2000^{o}R$ temperature. Tungsten-rhenium thermocouples placed around the perimeter showed there was a relatively cool region from the center of the spud, through the fuel portion and approximately 60% of the distance to the adjacent spud. In the cool region the temperature stabilized in the $500\text{-}1000^{o}R$ range while in the hot zone it remained in the $2000\text{-}3000^{o}R$. (These temperatures were in agreement with the phase measurements.) Along the zone interfaces there were severe temperature fluctuations.

The spuds were reoriented in an attempt to equalize the wall surface temperatures by putting the fuel rich zone toward the wall. It was also hoped that the new configuration would lead to greater instability because damping was occurring in about 50 milliseconds with only a few cavities active. Stability was easily obtained thus presenting an unsuitable test condition. Therefore, an unlike-doublet injector

was used since it was known to be inherently unstable. A limited-length cruiciform baffle designed to select the second tangential mode was used in conjunction with the liner. With the resonating cavities adjusted to the second tangential mode, a first tangential mode oscillation of low amplitude was observed in the chamber. When the cavities were tuned for the first tangential mode, the second tangential mode appeared in the chamber. A three-bladed baffle was used in place of the four-bladed design, and groups of cavities (using all the available resonating cavities) were tuned to eliminate the first and second tangential modes. This reduced the amplitude of both, but the first radial and several combined modes appeared. In summary, for this unlike injector the instability could not be damped with any combination of cavity tuning.

A combination of spuds from the like-on-like, which was stable under all conditions, and from the unlike impingement, which was extremely unstable, was tried in an effort to reach a marginal instability range which was necessary to determine the optimum placement of the resonating cavities at pressure or velocity nodes. However, the combined injector scheme was still unstable and more closely resembled the unlike tests.

Rather than continue in the quest for a proper rocket "test bed" for determining optimum circumferential locations for the acoustic dampers, attention was turned toward cold flow simulation. Perhaps one of the principal sources of difficulty in the hot firings was that the level of uniformity reached in higher thrust multi-element-injector designs can not be achieved in 16 spud motors. This would appear to be particularly true for the wall conditions where barrier coolant improves uniformity for the full scale combustors.

REFERENCES

1. Reardon, F.H. "A Brief Discussion of High Frequency Instability", Aerojet General Corp., TCR 9616/002, 3 Jan. 1962.

2. Barrere, M., et al, Rocket Propulsion, Elsevier Publishing Company, 1960, pg. 696-700.

3. Zucrow, M.J. "Combustion Oscillations in Liquid Bipropellant Rocket Motors", Purdue University: Presented at EAFB-RPL, 28 July 1965, under the auspices of the University of California, Los Angeles.

4. Sutton, G.P., Rocket Propulsion Elements - Third Edition, John Wiley and Sons, Inc., New York, pg. 254-256.

5. Weiss, R.R., "An Introduction to Combustion Instability in Liquid Propellant Rocket Engines", AFRPL-TR-66-50, July 1966.

6. Smith, R.P., and Sprenger, D.F., "Combustion Instability in Solid Propellant Rockets", 4th Symposium (International) on Combustion, 1952, pg. 893-906.

7. Crocco, L., "Aspects of Combustion Instability in Liquid Propellant Rockets", AFRS Journal; Part I, Vol. 21, p. 163, Nov. 1951; Part II, Vol.22 , p. 7, Jan. 1952.

8. Crocco, L., and Cheng, S.I., "Theory of Combustion Instability in Liquid Propellant Rocket Motors", AGARDograph No. 8, Butterworths Scientific Publications, Ltd., London, 1956.

9. Crocco, L, Grey, J., and Harrje, D.T., "Theory of Liquid Propellant Rocket Motors", Princeton University Aeronautical Engineering Report No. 550, 1 June 1961.

10. Crocco, L., "Theoretical Studies on Liquid Propellant Rocket Instability", 10th Symposium (International) on Combustion, 1964, pg. 1101-1128.

11. Priem, R.J., and Guentert, D.C., "Combustion Instability Limits Determined by a Nonlinear Theory and a One-Dimensional Model", NASA TN D-1409, Oct. 1962.

12. Blackman, A.W., "Effect of Nonlinear Losses on the Design of Absorbers for Combustion Instabilities", ARS Journal, Vol. 30, No. 11, Nov. 1960.

13. Garrison, G.D., "A Study of the Suppression of Combustion Oscillation with Mechanical Damping Devices", Pratt and Whitney Aircraft, FR-1922, 15 July 1966.

REFERENCES - continued

14. Crocco, L., Harrje, D.T., Sirignano, W.A., et al, "Nonlinear Aspects of Combustion Instability in Liquid Propellant Rocket Motors", Princeton University Department of Aerospace and Mechanical Sciences Report 553-f, 1 June 1966.

15. Heat Flux System Model 1000A Instruction Manual, Thermo Systems, Inc.

16. Hinze, J.O. Turbulence, McGraw-Hill Book Company, Inc., New York, p. 77.

17. McAdams, W.H., Heat Transmission, McGraw-Hill Book Company, Inc., New York, p. 155.

18. Crocco, L., Harrje, D.T., Sirignano, W.A., et al, "Nonlinear Aspects of Combustion Instability in Liquid Propellant Rocket Motors", Princeton University Department of Aerospace and Mechanical Sciences Report 553-g, 1 June 1967.

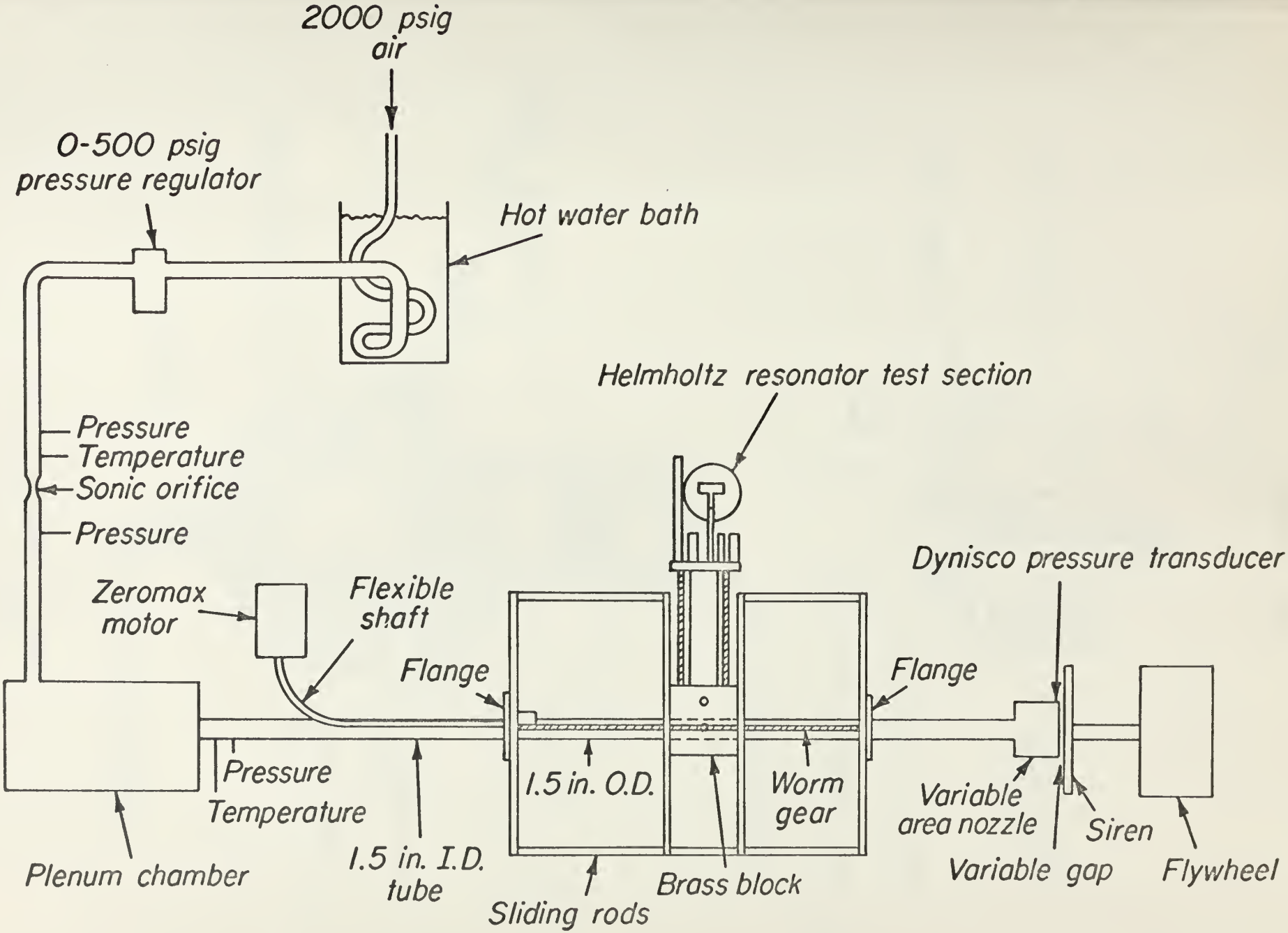


Figure 1

Test apparatus

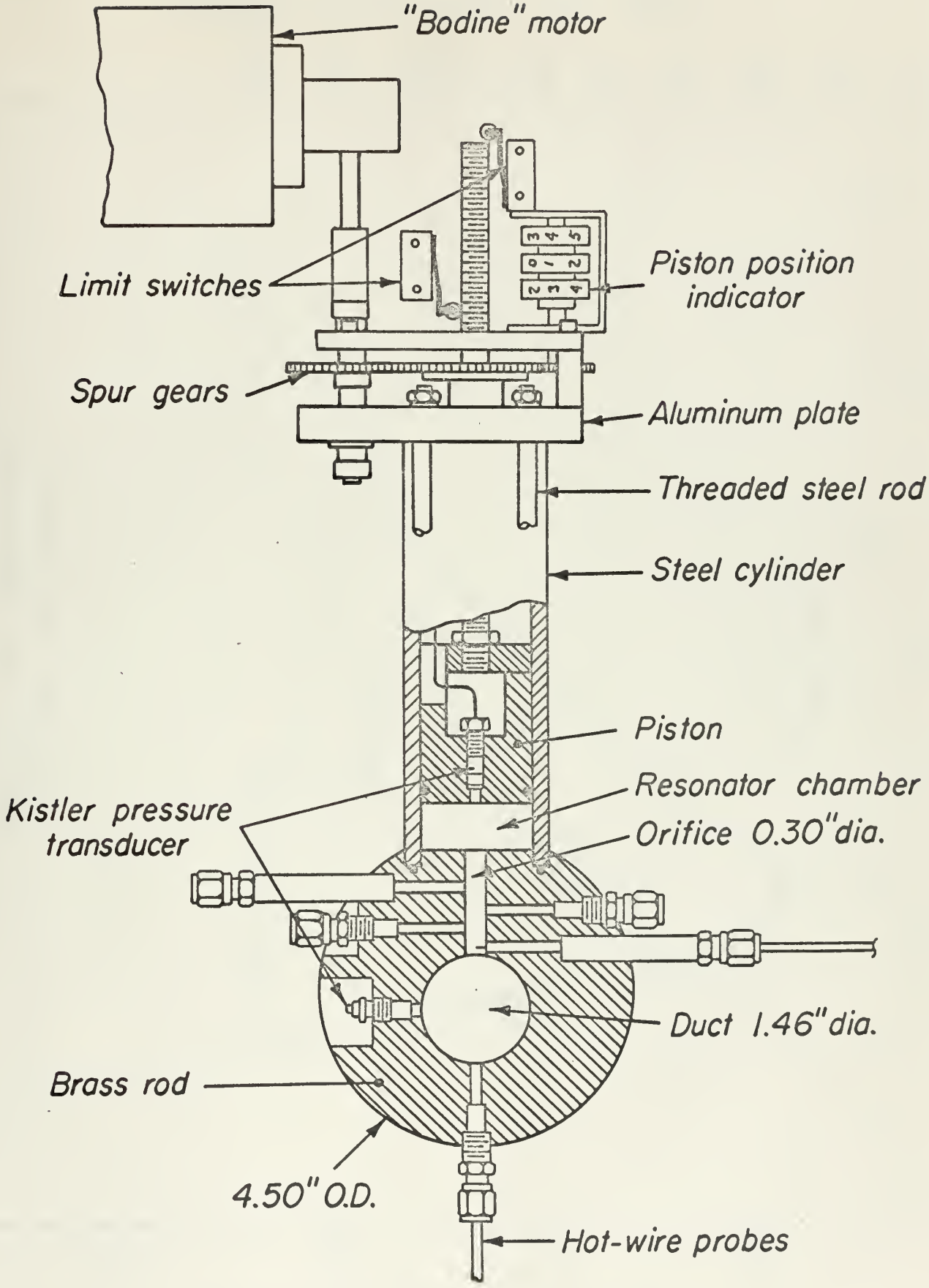


Helmholtz resonator section

Figure 2

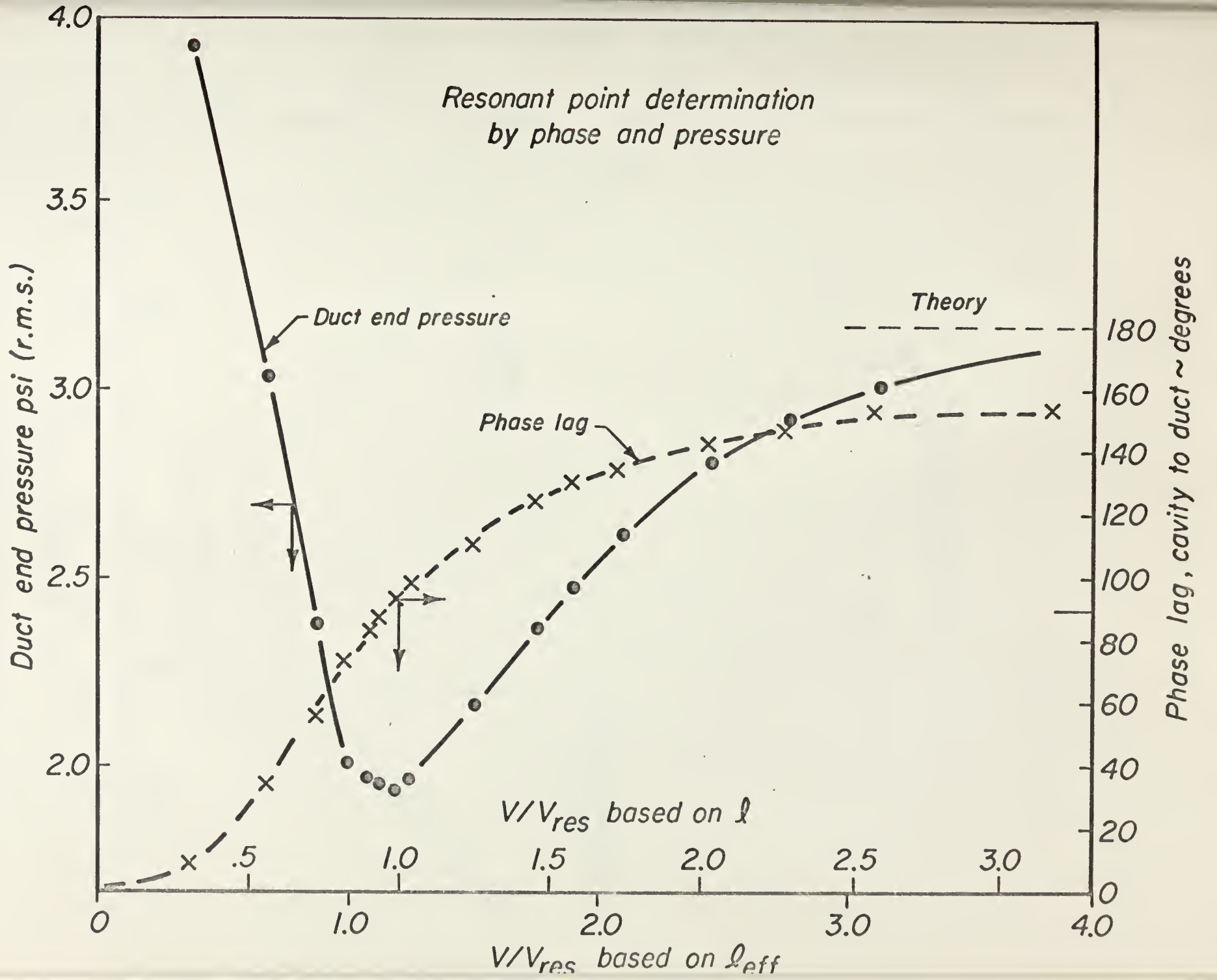
Resonant point determination
by phase and pressure
Duct end pressure
Phase lag
Theory
Duct end pressure psi (r.m.s.)
Phase lag, cavity to duct ~ degrees
4.0
3.5
3.0
2.5
2.0
180
160
140
120
100
80
60
40
20
0
.5
1.0
1.5
2.0
2.5
3.0
V/V_res based on ℓ
0
1.0
2.0
3.0
4.0
V/V_res based on ℓ_eff

Figure 3

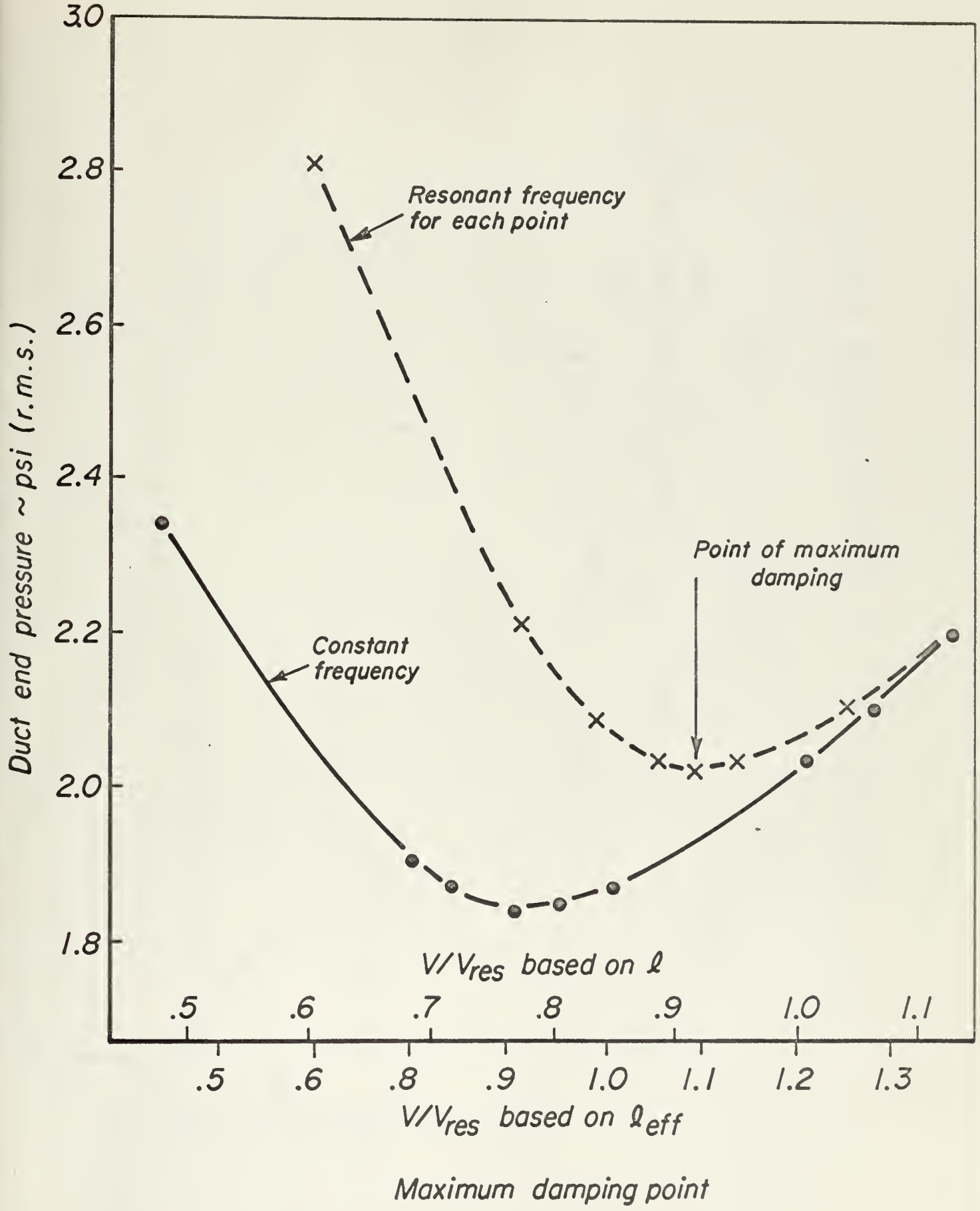
3.0
2.8
2.6
2.4
2.2
2.0
1.8
Duct end pressure ~ psi (r.m.s.)
Resonant frequency for each point
Point of maximum damping
Constant frequency
V/V_res based on ℓ
.5
.6
.7
.8
.9
1.0
1.1
.5
.6
.8
.9
1.0
1.1
1.2
1.3
V/V_res based on ℓ_eff
Maximum damping point

Figure 4

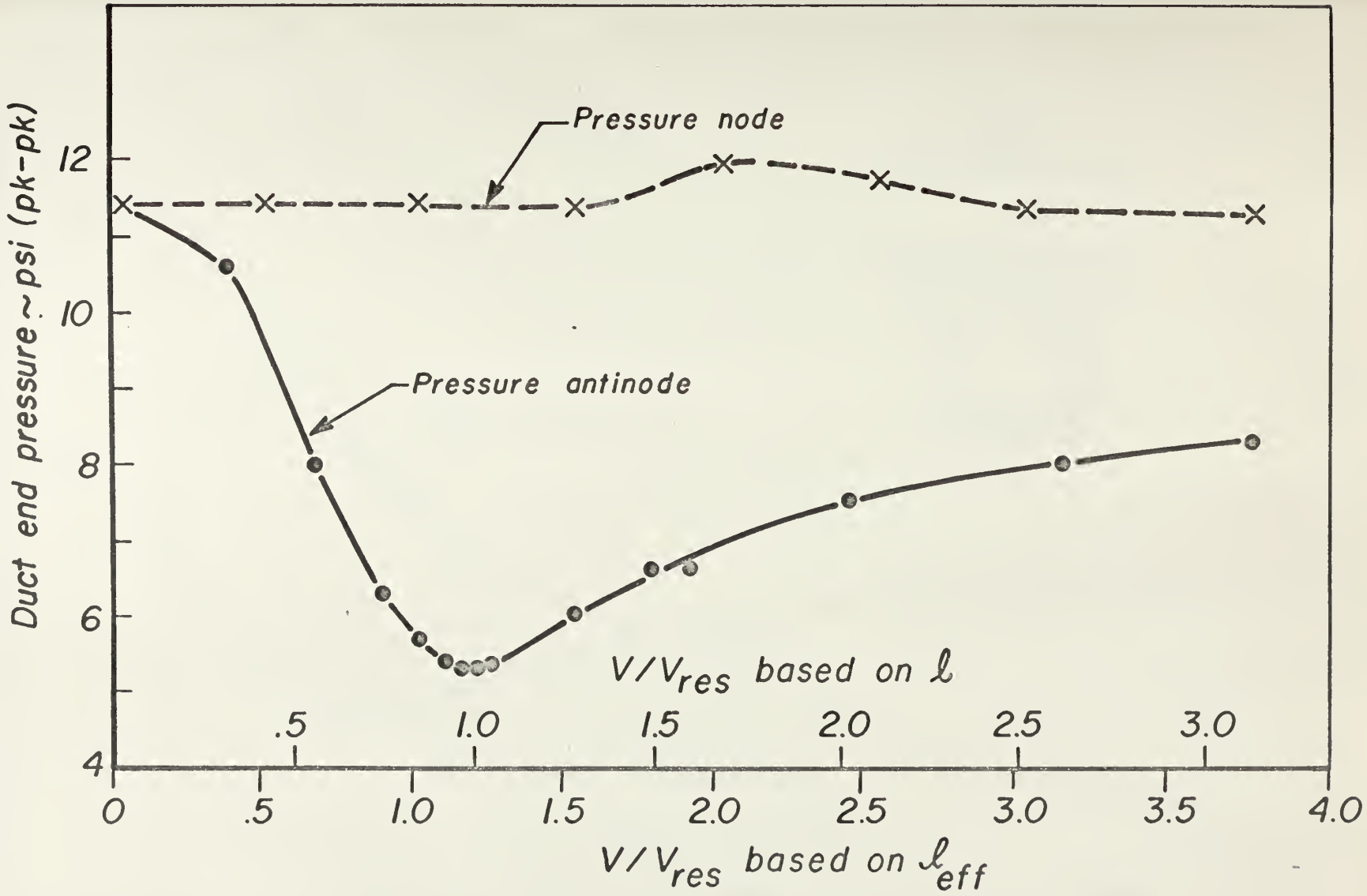


Damping effect at pressure node & antinode

Figure 5

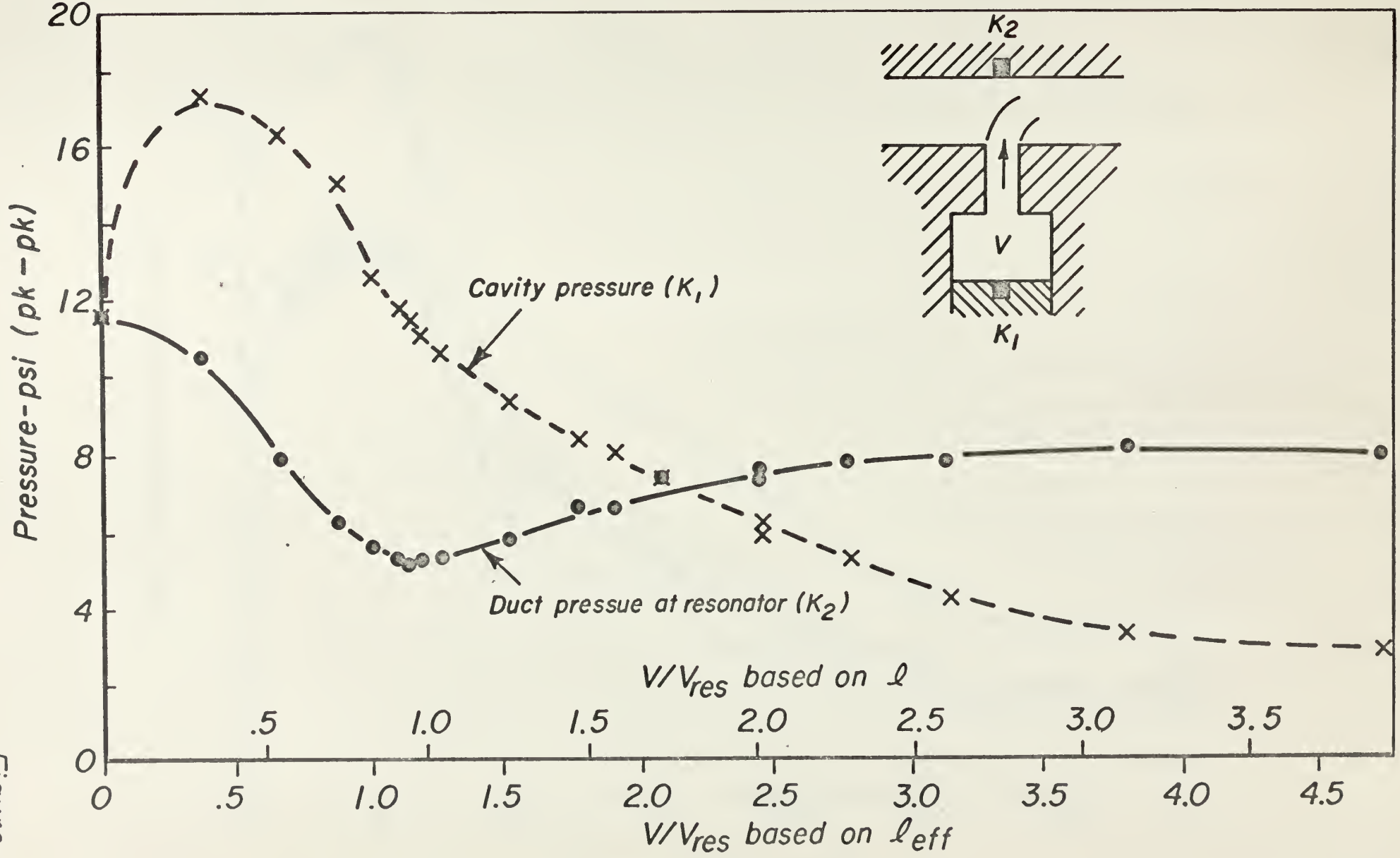


Figure 60

Cavity and duct pressures vs resonator volume variations
@ 416 Hz steady-state pressure 55 psia

Preliminary data on cavity pressure vs. resonator volume

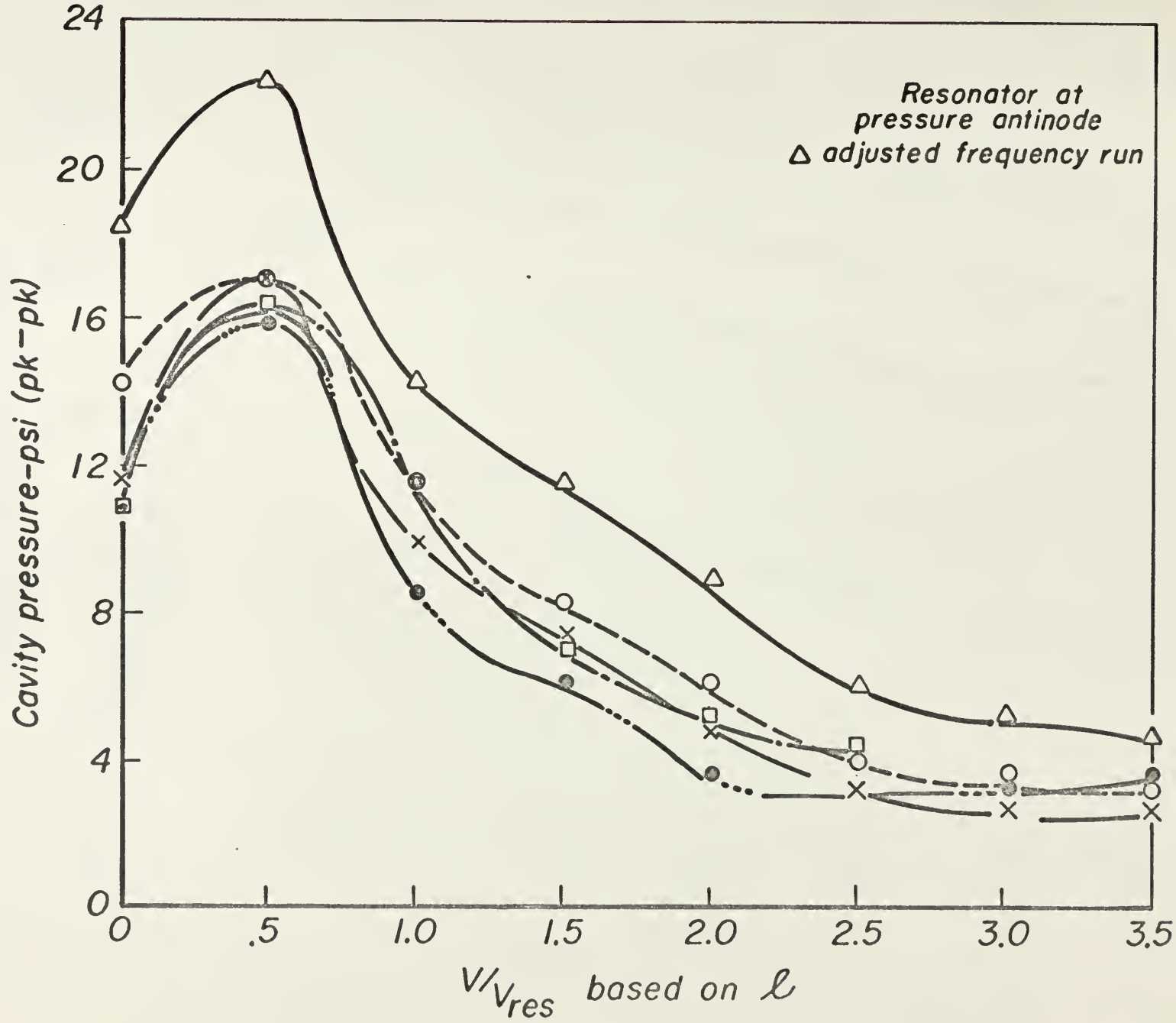


Figure 69

Preliminary data on orifice velocity vs. resonator volume

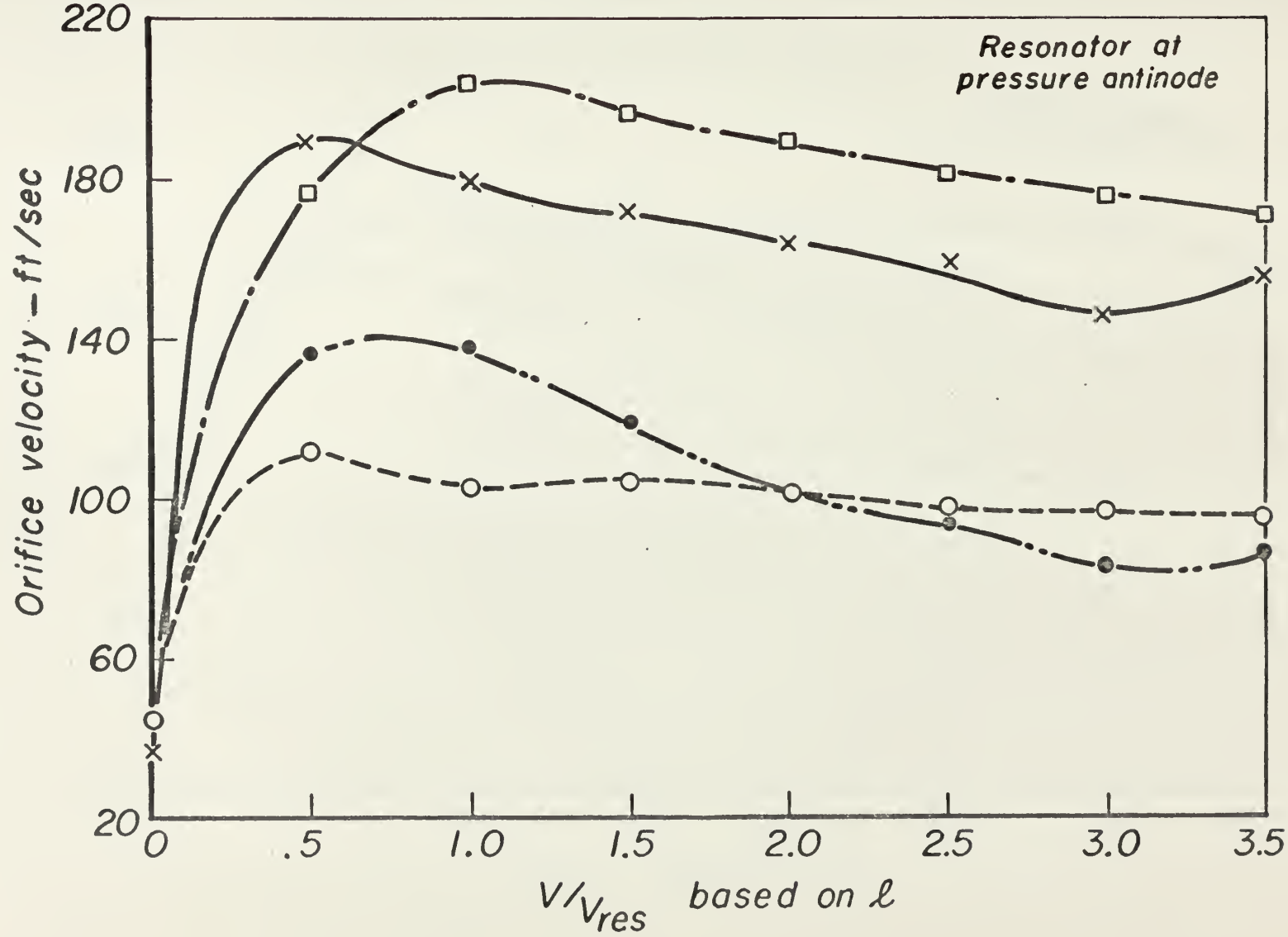


Figure 7

*Preliminary data on unsteady duct velocity vs. resonator volume*

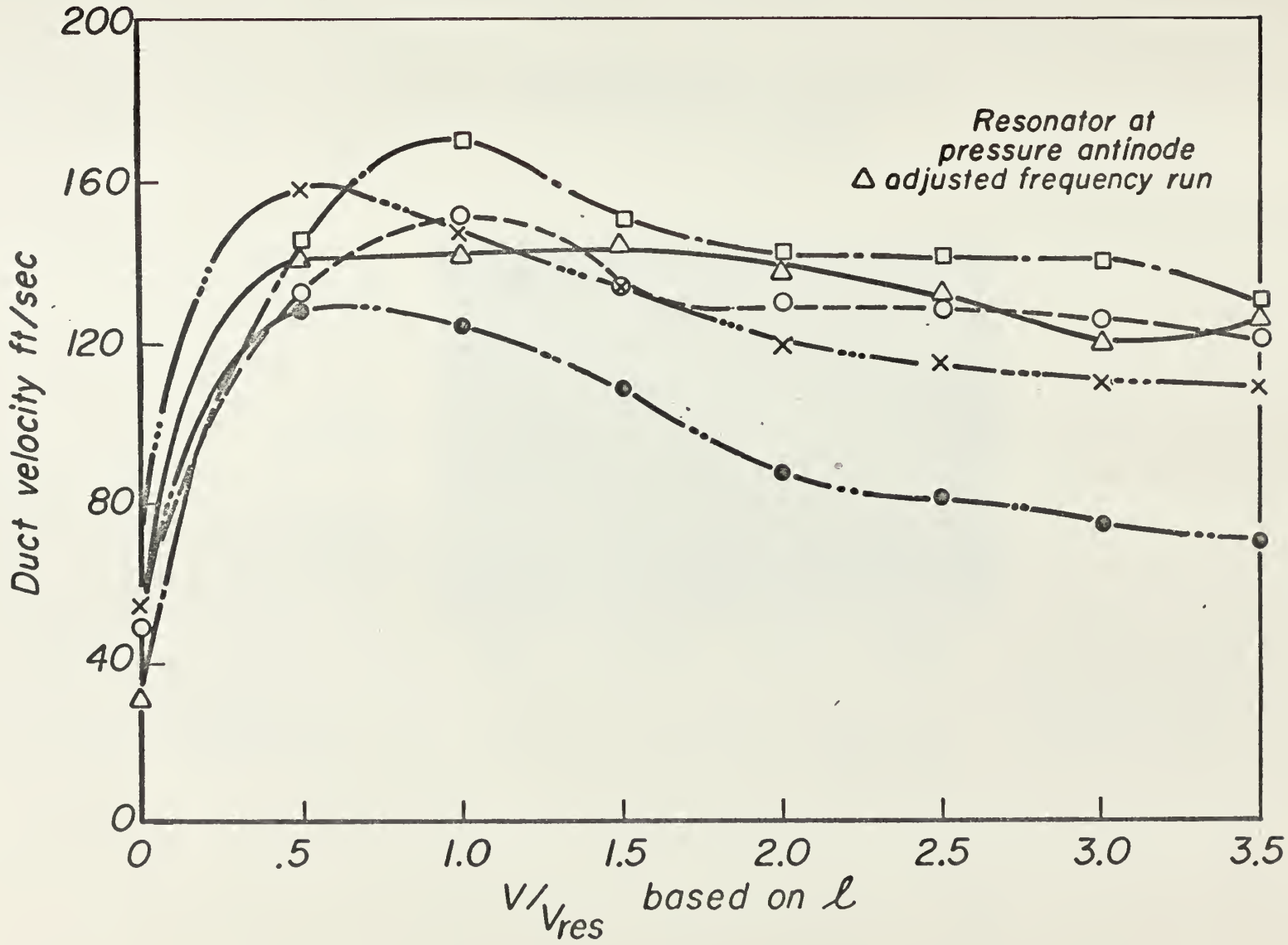


Figure 8

Oscilloscope photograph
of wave shapes

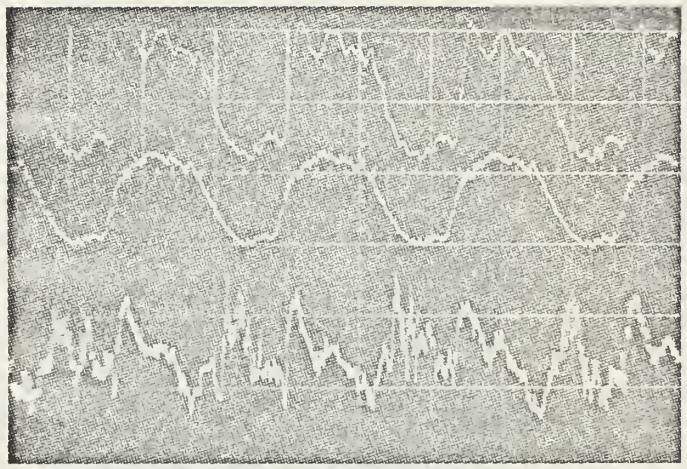


0.0 × resonant cavity volume

Figure 9

Oscilloscope photographs of wave shapes

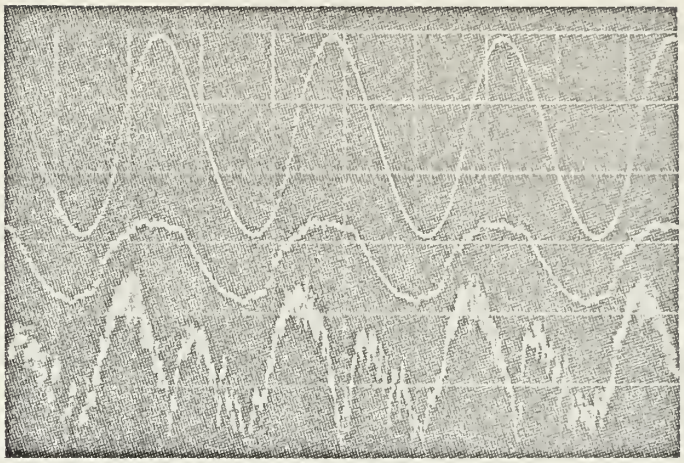


0.5 × resonant cavity volume

Figure 10

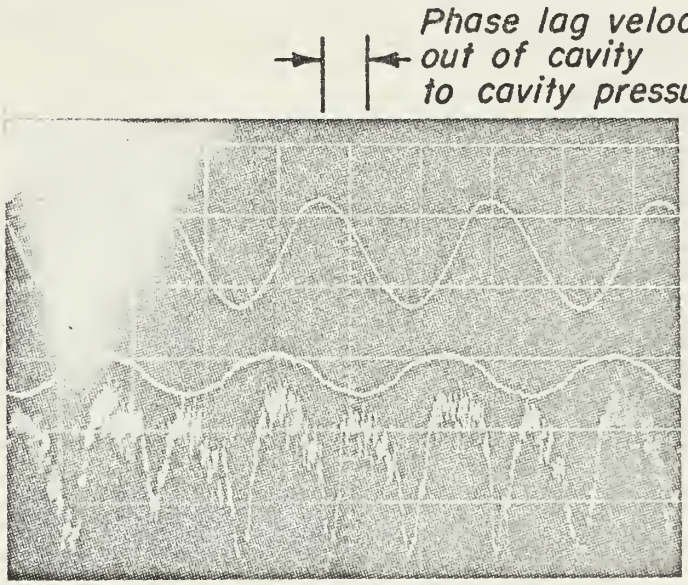


1.0 × resonant cavity volume

Figure 11

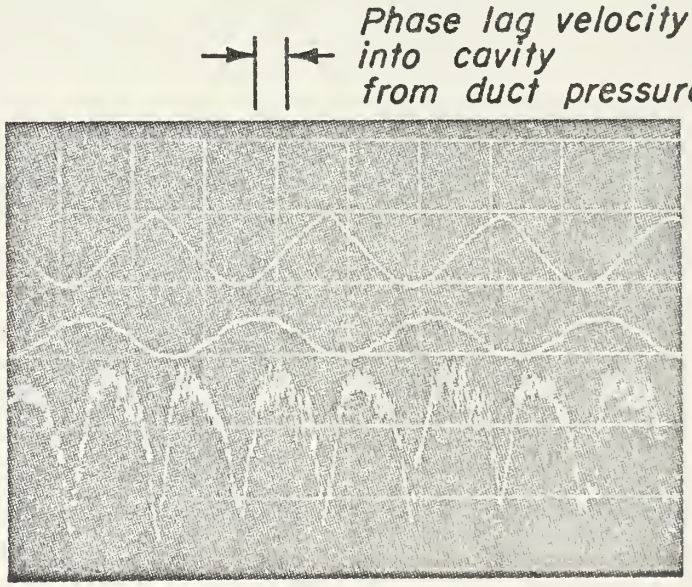


1.5 × resonant cavity volume

Figure 12

Oscilloscope photographs
of wave shapes

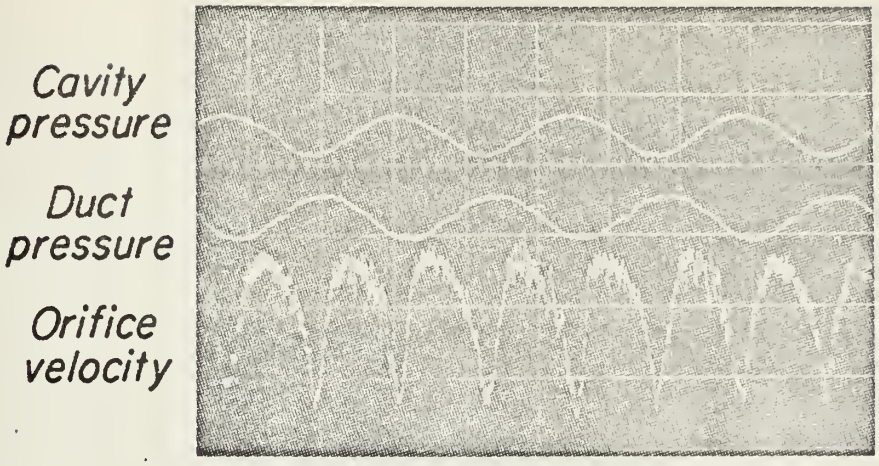


2.0 × resonant cavity volume

Figure 13

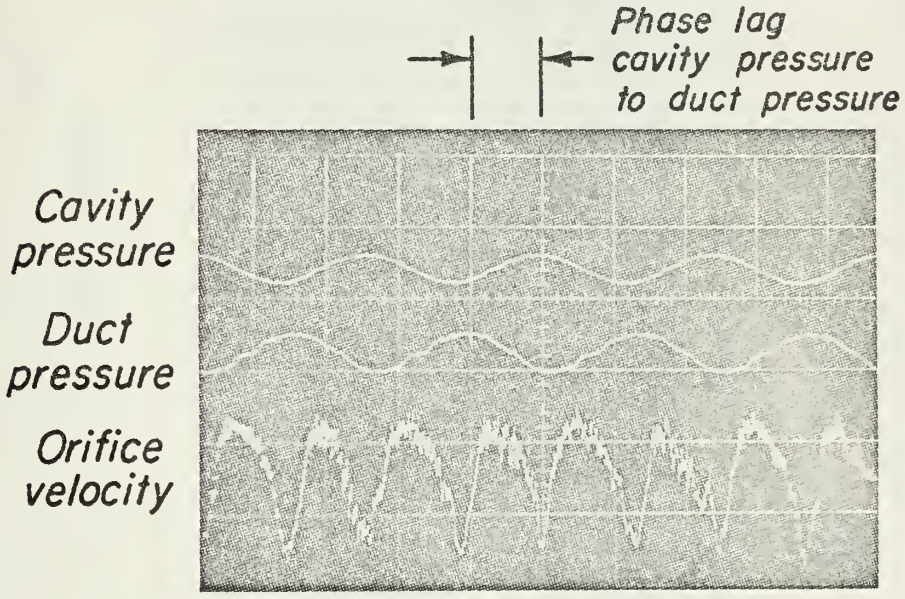


2.5 × resonant cavity volume

Figure 14

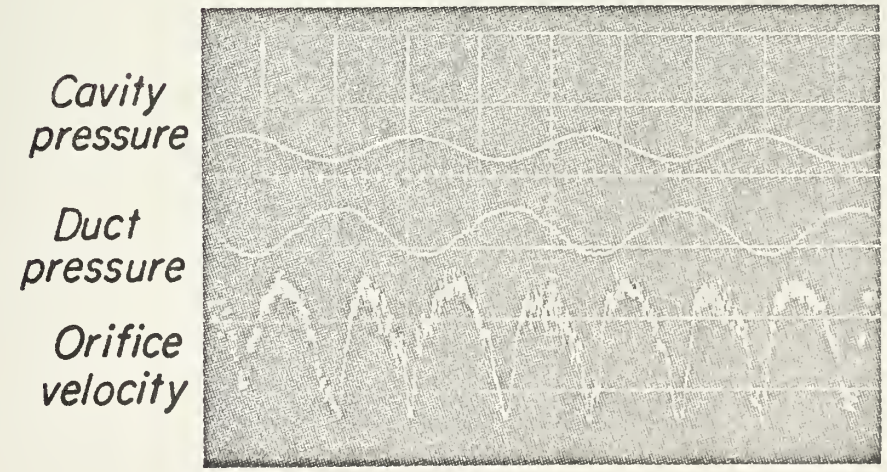


3.0 × resonant cavity volume

Figure 15

Oscilloscope photograph
of wave shapes

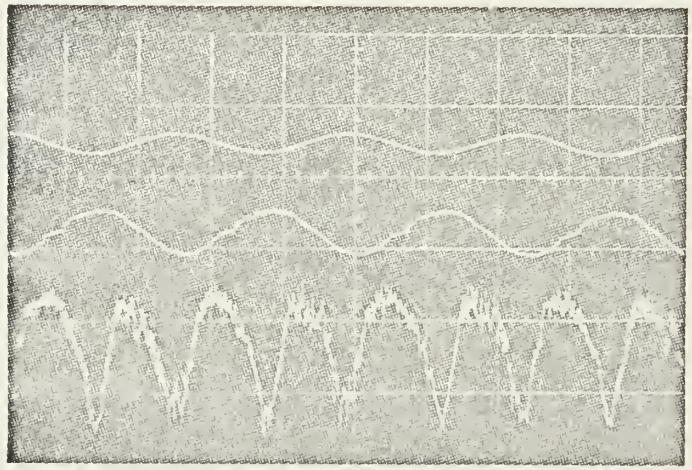


3.5 × resonant cavity volume

Figure 16

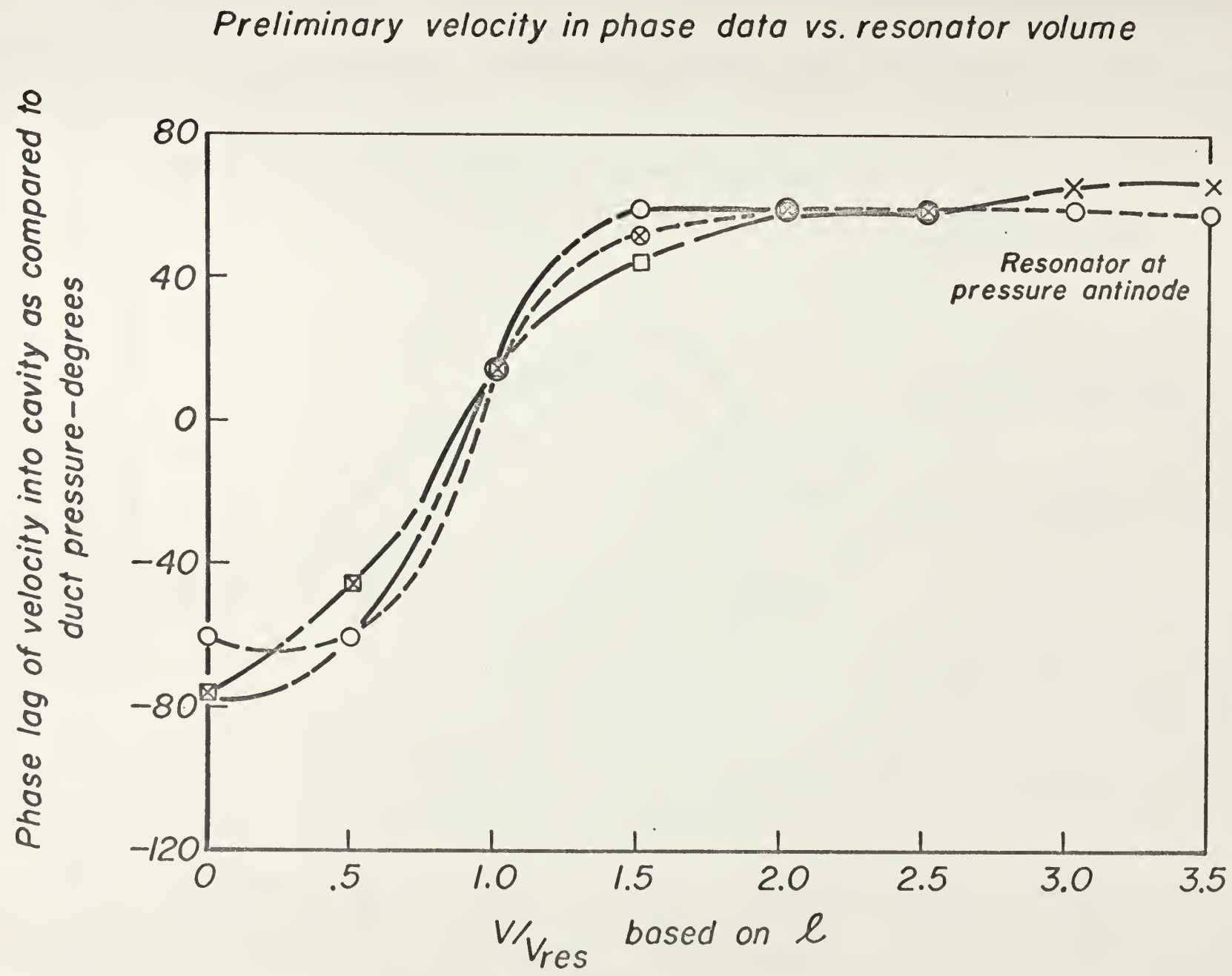
Preliminary velocity in phase data vs. resonator volume
Phase lag of velocity into cavity as compared to duct pressure-degrees
80
40
0
-40
-80
-120
0
.5
1.0
1.5
2.0
2.5
3.0
3.5
V/Vres based on ℓ
Resonator at pressure antinode

Figure 17

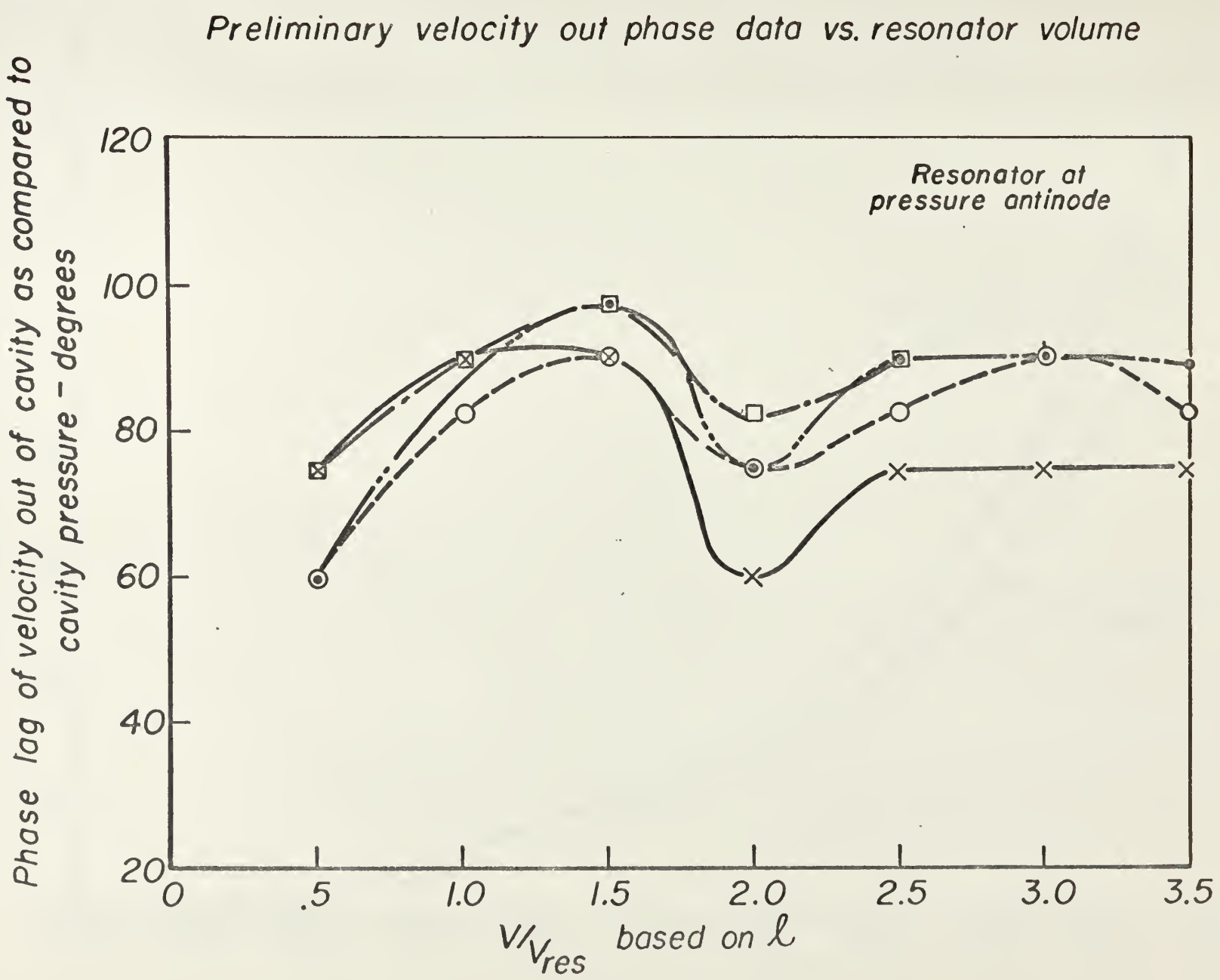
Preliminary velocity out phase data vs. resonator volume
Phase lag of velocity out of cavity as compared to cavity pressure - degrees
120
100
80
60
40
20
Resonator at pressure antinode
0
.5
1.0
1.5
2.0
2.5
3.0
3.5
V/V_res based on ℓ

Figure 18

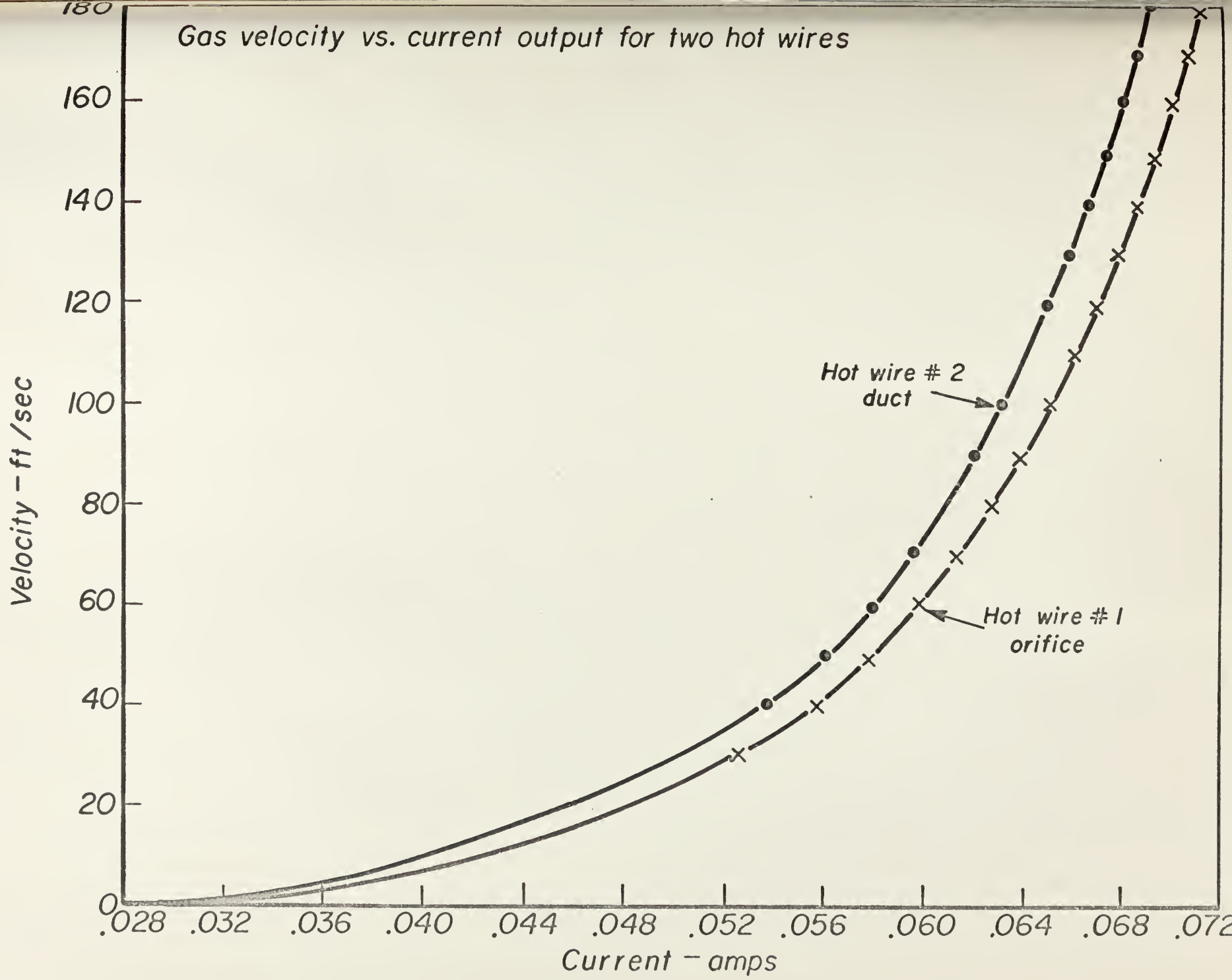
Gas velocity vs. current output for two hot wires
Velocity – ft /sec
180
160
140
120
100
80
60
40
20
0
.028
.032
.036
.040
.044
.048
.052
.056
.060
.064
.068
.072
Current – amps
Hot wire # 2
duct
Hot wire # 1
orifice

Figure A-1